BIOCHEMISTRY
including biophysical chemistry & molecular biology
Article

Biochemistry **2009,** *48,* 11357–11369 11357
DOI: 10.1021/bi9015082

Kinetic Mechanism for the Flipping and Excision of 1,N^6-Ethenoadenine by Human Alkyladenine DNA Glycosylase†

Abigail E. Wolfe and Patrick J. O'Brien*

Department of Biological Chemistry, University of Michigan, Ann Arbor, Michigan 48109-5606

Received August 27, 2009; Revised Manuscript Received October 21, 2009

ABSTRACT: Human alkyladenine DNA glycosylase initiates the repair of a wide variety of alkylated and deaminated purine lesions in DNA. In this study, we take advantage of the natural fluorescence of the 1,N^6-ethenoadenosine (εA) lesion and report a kinetic analysis of binding, nucleotide flipping, base excision, and product release. The transient changes in the fluorescence of εA revealed the existence of two distinct complexes that are formed prior to the hydrolysis step. An initial recognition complex forms rapidly and is characterized by partial disruption of the stacking interactions of the lesioned base. Subsequently, a very stable extrahelical complex is formed in which the εA lesion is strongly quenched by interactions in the AAG active site pocket. Our results indicate that DNA binding and base flipping take place on the millisecond to second time scale. N-Glycosidic bond cleavage is much slower, taking place on the minute time scale. A pulse−chase experiment was used to demonstrate that even for the tightly bound εA substrate, the extrahelical complex is not fully committed to excision. Nevertheless, flipping of εA is highly favorable, and we calculate that the equilibrium constant for flipping is ∼1300. This kinetic mechanism has important biological implications. First, two-step binding provides multiple opportunities to discriminate between damaged and undamaged nucleotides. Second, a rapid equilibrium flipping mechanism maximizes specificity for damaged versus undamaged bases, since undamaged bases generally form stronger base pairs than damaged bases. Finally, the highly favorable equilibrium for flipping of εA ensures that εA removal is independent of sequence context and highly efficient despite the relatively slow rate of N-glycosidic bond hydrolysis.

The nucleobases of DNA are susceptible to spontaneous chemical modification, including oxidation and alkylation. Failure to repair the resulting DNA lesions can result in mutations or in some cases cell death. The majority of simple base lesions are repaired via the base excision repair (BER)[1] pathway (*1*). This pathway is initiated by a DNA repair glycosylase that is responsible for finding the damaged site and catalyzing the hydrolysis of the N-glycosidic bond. In the case of a monofunctional DNA glycosylase, this results in the release of the lesioned base and the formation of an abasic site in the DNA. The abasic site is further processed to nick the DNA backbone and remove the abasic sugar residue. Repair synthesis uses the intact strand as a template to ensure incorporation of the correct nucleotide, and the nick is ultimately sealed by DNA ligase.

The human enzyme, alkyladenine DNA glycosylase (AAG), is responsible for repairing a diverse set of alkylated and oxidized purines, including purines alkylated at the N7 and N3 positions, and the deaminated purines hypoxanthine (Hx) and oxanine (refs *2* and *3* and references cited therein). Chemical structures of damaged and undamaged adenine bases are shown in Scheme 1. AAG also recognizes the bulkier alkylation adduct, 1,N^6-ethenoadenosine (εA), that can be formed from lipid peroxidation products and exposure to exogenous agents such as urethane and vinyl chloride (*4*, *5*). This lesion is highly mutagenic in mammalian cells and leads to misincorporation of all possible nucleotides if it is replicated prior to repair (*6*, *7*). AAG is the only known human glycosylase that catalyzes the excision of εA, but an alternative direct reversal pathway has recently been discovered in which εA can be directly oxidized to restore the adenine base by AlkB family members (*8*). This backup pathway may account for the observation that mice lacking AAG remain viable (*9*, *10*). Nevertheless, mice lacking AAG have decreased rates of repair of εA and are unable to tolerate the burden of increased levels of DNA alkylation (*11*, *12*).

Structural and biochemical studies have provided considerable insight into the mechanism by which AAG recognizes and excises damaged bases and have suggested the minimal mechanism that is illustrated in Figure 1. Given the low frequency with which sites of DNA damage occur, initial binding is most likely to occur at an undamaged site. AAG uses nonspecific binding interactions to scan DNA in the search for sites of damage (*13*). Once a damaged nucleotide is encountered, it must be flipped out of the duplex by 180° into the enzyme active site where lesion recognition and N-glycosidic bond hydrolysis can occur (*14*−*16*). The excised base is released, and the abasic nucleotide must disengage from the active site in the reverse of the flipping step. The nonspecifically

†This work was supported in part by a fellowship from the University of Michigan Chemical Biology Interface training grant to A.E.W., a Faculty Research Grant from the Horace H. Rackham School of Graduate Studies to P.J.O., and by a grant from the National Institutes of Health to P.J.O. (CA122254).

*To whom correspondence should be addressed: Department of Biological Chemistry, University of Michigan Medical School, 1150 W. Medical Center Dr., Ann Arbor, MI 48109-5606. Phone: (734) 647-5821. Fax: (734) 764-3509. E-mail: pjobrien@umich.edu.

[1]Abbreviations: AAG, alkyladenine DNA glycosylase, also known as methylpurine DNA glycosylase (MPG) and 3-methyladenine DNA glycosylase; BER, base excision repair; BSA, bovine serum albumin; εA, 1,N^6-ethenoadenine; Fpg, formamidopyrimidine DNA glycosylase; Hx, hypoxanthine (the base moiety of inosine); *I*, ionic strength; NaHEPES, sodium *N*-(2-hydroxyethyl)piperazine-*N*′-2-ethanesulfonate; NaMES, sodium 2-(*N*-morpholino)ethanesulfonate; PAGE, polyacrylamide gel electrophoresis.

Published on Web 11/02/2009

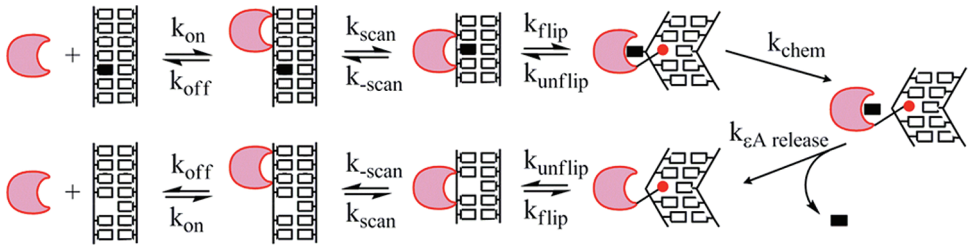

FIGURE 1: Minimal mechanism for AAG-catalyzed nucleotide flipping and base excision. AAG (crescent) binds nonspecifically to DNA and rapidly slides in search of DNA damage. Once a lesion (filled rectangle) is encountered in an initial damage recognition complex, it can be flipped out into the active site to form the specific recognition complex. In this specific complex, the DNA is bent, the damaged nucleotide is flipped out by 180°, and Y162 (red circle) is intercalated into the DNA to take the place of the extrahelical lesion (*15*, *16*). From this specific complex, AAG catalyzes hydrolysis of the N-glycosidic bond (k_{chem}). The lesion base is subsequently released ($k_{\varepsilon Arelease}$). The abasic product is an inhibitor of AAG, so presumably the sugar can be stably bound in a flipped-out conformation analogous to the abasic pyrrolidine conformation observed by X-ray crystallography (*15*). Dissociation of AAG from the abasic product requires rotation of the abasic sugar back into the duplex (k_{unflip}). From the less tightly bound complex, AAG can translocate along the DNA in search of additional sites of damage and can ultimately dissociate (k_{off}).

Scheme 1

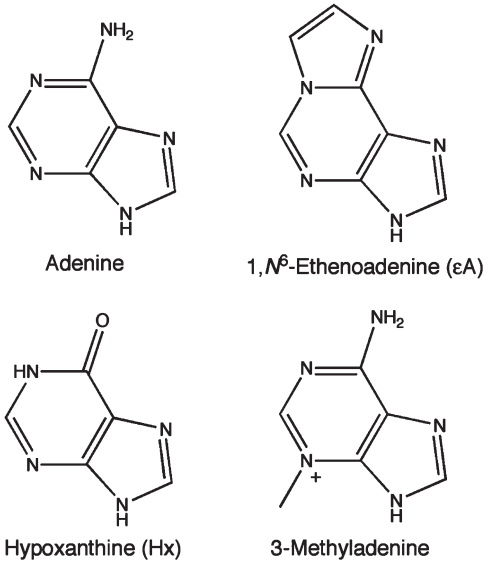

bound AAG is able to diffuse away along the duplex in search of additional sites of damage and eventually can be released into solution. The rates of DNA binding and nucleotide flipping have not previously been measured for AAG but are critical in understanding how the enzyme recognizes a wide variety of damaged nucleotides. Several previous studies have used intrinsic protein fluorescence or the incorporation of fluorescent reporter groups into DNA to investigate the kinetics of DNA binding and nucleotide flipping by other families of DNA glycosylases (*17*−*22*). Together with studies of other DNA-modifying enzymes, these studies have begun to address the fundamental, common features of nucleotide flipping enzymes (*14*).

There is, however, circumstantial evidence that the requirement for nucleotide flipping provides a barrier to the excision of damaged bases by AAG (*2*, *23*, *24*). For example, the rate of excision of a given lesion paired with different opposing bases is inversely proportional to the base pairing stability [e.g., 7-methylguanine (7mG) is excised from a 7mG·T mismatch 50-fold faster than it is removed from a stable 7mG·C pair]. Since AAG does not make specific contacts with the opposing base, this observation is best explained by an AAG complex in which the lesion can still form a hydrogen bond with the opposing base (*2*). In addition, rates of repair vary widely for a given lesion

Scheme 2

TEC 5′-CGATAGCATCCT**E**CCTTCTCTCCAT
3′-GCTATCGTAGGATGGAAGAGAGGTA

AEA 5′-CGATAGCATCAA**E**AATTCTCTCCAT
3′-GCTATCGTAGTTTTTAAGAGAGGTA

base pair in different local sequence contexts (*25*). The effect of sequence context is most pronounced for excision of Hx (*25*, *26*). For example, rates of excision of Hx from different regions of a polyA tract vary by almost 2 orders of magnitude (*26*). An early report mentioned that excision of εA is also sensitive to its position in a poly(A) tract (*27*), but subsequent studies found little or no sequence context effects for the excision of εA by AAG (*25*, *26*). We were interested in learning whether nucleotide flipping is rapid, as has been observed for other DNA glycosylases (*17*, *19*−*22*), or whether the flipping step might be significantly slower than the base excision step.

Since εA is known to be fluorescent and very sensitive to its local environment (*28*), we investigated the possibility of directly monitoring the dynamics of DNA binding and nucleotide flipping for this biologically relevant DNA adduct. We combined single-turnover and multiple-turnover glycosylase assays with stopped-flow fluorescence measurements to characterize the kinetic mechanism for AAG-catalyzed excision of εA. We show that binding of AAG to the DNA is fast compared to the other steps and that binding is reversible. We present evidence that nucleotide flipping is rapid and highly favorable and that the excised lesion is rapidly released. These fast conformational changes, with relatively slow base excision, are integral to the ability of AAG to discriminate between damaged and undamaged nucleotides.

MATERIALS AND METHODS

Purification of Human Recombinant Protein. The catalytic domain of human AAG that lacks the first 79 amino acids was expressed in *Escherichia coli* and purified as previously described (*29*). The concentration of active AAG was determined by burst analysis, using an inosine-containing oligonucleotide substrate, as previously described (*13*, *30*).

Synthesis and Purification of Oligodeoxynucleotides. The 25mer oligonucleotides or the constituent phosphoramidites were obtained from commercial sources and contained a central lesion that was placed opposite of a T. The sequences are given in Scheme 2. Oligonucleotides containing only normal

deoxynucleotides or deoxyinosine were synthesized and deprotected with standard phosphoramidite chemistry, whereas those containing a single εA lesion were synthesized and deprotected using Ultra-Mild chemistry according to the supplier's recommendations. The εA-containing oligonucleotides were synthesized by the W. M. Keck Facility at Yale University (New Haven, CT), or the phosphoramidite was obtained from Glen Research and incorporated using an ABI 394 DNA synthesizer. The oligonucleotides were desalted using Sephadex G-25 and purified using denaturing polyacrylamide gel electrophoresis as previously described (*13*). Oligonucleotides for gel-based assays were labeled on the lesion-containing strands with a 5′-fluorescein (6-fam) label. The concentrations of the single-stranded oligonucleotides were determined from the absorbance at 260 nm, using the calculated extinction coefficients for all oligonucleotides except those containing εA. For εA-containing oligonucleotides, the extinction coefficient was calculated for the same sequence with an A in place of the εA and corrected by subtracting 9400 M^{-1} cm^{-1} to account for the weaker absorbance of εA versus that of A (*31*). The lesion-containing oligonucleotides were annealed with a 1.1-fold excess of the complement by being heated to 90 °C and cooled slowly to 4 °C.

Steady-State Fluorescence Measurements. Fluorescence emission spectra were recorded with a PTI QuantaMaster fluorometer controlled by FeliX software. For εA fluorescence, an excitation wavelength of 320 nm (6 nm band-pass) was used and the total fluorescence was measured at emission wavelengths from 350 to 500 nm (6 nm band-pass). Samples (200 μL) of 400 nM εA-containing DNA were prepared in the standard buffer [50 mM NaMES (pH 6.5), 100 mM NaCl, 1 mM EDTA, and 1 mM DTT], and spectra were recorded at 25 °C. To determine the steady-state fluorescence of εA-containing DNA bound to AAG, the spectra were recorded within 1 min. No significant excision of εA occurs during this time.

Single-Turnover Excision of εA Monitored by Fluorescence. Since εA is strongly quenched in duplex DNA and when bound to AAG, we were able to follow the release of εA into solution by the increase in fluorescence. Single-turnover glycosylase assays were performed in the standard buffer at 25 °C with 400 nM DNA duplex and 1.2−2.4 μM AAG. A full emission spectrum was recorded at various times between 2 and 120 min. The greatest change in fluorescence occurred at 410 nm; therefore, this wavelength was chosen to follow the release of εA into solution. The fluorescence at 410 nm was used to determine the fraction of εA product [fraction product = $(F_t - F_0)/F_{max}$, where F_t is the fluorescence at time t, F_0 is the initial fluorescence at time zero, and F_{max} is the maximal fluorescence change]. This normalization gives fraction product values between 0 and 1. These data were fit by a single-exponential equation using nonlinear least-squares regression with Kaleidagraph (Synergy Software), in which k_{obs} is the rate constant, t is the time, and A is the amplitude (eq 1).

$$\text{fraction product} = A(1 - e^{-k_{obs}t}) \quad (1)$$

The single-turnover rate constant was determined at a saturating concentration of AAG, and this was confirmed by the observation of the same rate constant at two different concentrations of AAG (see the Supporting Information). Under these conditions, the observed rate constant is equal to the maximal single-turnover rate constant ($k_{obs} = k_{max}$).

Glycosylase Activity Assay. We also measured single-turnover glycosylase activity with the standard glycosylase activity assay that utilizes abasic site cleavage by NaOH followed by DNA separation on a denaturing PAGE gel (*13*, *29*). Fluorescein-labeled DNA substrates (20−100 nM) were prepared in the standard buffer with 0.1 mg/mL BSA added. The reactions were initiated by the addition of 100−400 nM AAG and the mixtures incubated at 25 °C. At various time points, a sample from the reaction was removed and quenched in 2 equiv of 0.3 M NaOH, giving a final hydroxide concentration of 0.2 M. The abasic sites were cleaved by heating at 70 °C for 10 min. Samples were mixed with an equal volume of formamide/EDTA loading buffer and heated for 3 min at 70 °C before being loaded onto a 12 to 15% polyacrylamide gel. Gels were scanned with a Typhoon Imager (GE Healthcare) to detect the fluorescein label via excitation at 488 nm, and emission was measured with a 520BP40 filter. The gel bands were quantified using ImageQuant TL (GE Healthcare). The data were converted to fraction product [fraction Product = product/(product + substrate)] and then fit by a single exponential (eq 1). The observed rate constant for the single-turnover reaction was independent of the concentration of AAG, indicating that the maximal rate constant was measured [$k_{obs} = k_{max}$ (see the Supporting Information)].

Stopped-Flow Kinetics. Pre-steady-state kinetic experiments were performed on a Hi-Tech SF-61DSX2 instrument, controlled by Kinetic Studio (TgK Scientific). The fluorescence of εA was measured using an excitation wavelength of 320 nm and a WG360 long-pass emission filter. The concentrations that are given for enzyme and substrate are those obtained after mixing equal volumes in the stopped-flow instrument. The reactions were followed for either 2 or 10 s to monitor initial binding events occurring before the base excision step could occur. Binding of AAG to εA-containing DNA was measured by mixing a constant concentration of DNA with increasing concentrations of AAG. Experiments were performed with either 0.15 or 0.5 μM DNA after mixing, and final concentrations of AAG of up to 8 μM. Three traces were averaged together at each concentration, which revealed two phases. The traces were fit by a double exponential (eq 2)

$$F = C - Y(1 - e^{-k_{1,obs}t}) - Z(1 - e^{-k_{2,obs}t}) \quad (2)$$

where F is the εA fluorescence as a function of time, C is the fluorescence of the free DNA, Y is the change in fluorescence of the first intermediate, and Z is the change in fluorescence of the second intermediate. The observed rate constants for the first and second steps are designated $k_{1,obs}$ and $k_{2,obs}$, respectively (eq 2).

It is possible to relate these observed rate constants to the microscopic rate constants in Scheme 3, with a bimolecular binding step followed by a unimolecular conformational change that occurs prior to the chemical step. The initial binding step appears to be reversible (see below), and therefore, the observed rate constant is given by the sum of the association and dissociation steps in Scheme 3 ($k_{1,obs} = [AAG]k_1 + k_{-1}$). It should be noted that this equation applies when [E] ≫ [S]. Under our conditions, the enzyme was in only modest excess (2−7-fold). Nevertheless, the resulting values of k_1 are in reasonably good agreement with the values measured by mixing equimolar

Scheme 3

$$E + S \underset{k_{-1}}{\overset{k_1}{\rightleftharpoons}} E\cdot S \underset{k_{-2}}{\overset{k_2}{\rightleftharpoons}} E\cdot S'$$

solutions of enzyme and substrate (see below). We suggest that the unimolecular step corresponds to nucleotide flipping. Since this is an approach to equilibrium, the observed rate constant is equal to the sum of the rate constants for the forward and reverse flipping steps ($k_{2,obs} = k_2 + k_{-2}$). Substrate dissociation experiments, measured by a pulse−chase method, suggest that k_2 is much greater than k_{-2}, indicating that $k_{2,obs}$ is approximately equal to k_2, the microscopic rate constant for flipping.

Rapid binding and weak fluorescence made it difficult to fully analyze the binding step under conditions with a true excess of enzyme over substrate; therefore, we also performed mixing experiments in which a 1:1 concentration ratio of DNA to AAG was maintained (0.15−1.5 μM). Three traces were averaged together at each concentration, and they were fit by eq 3

$$F = C + Y\left(\frac{E_0^2 k_1 t}{1 + E_0 k_1 t}\right) - Z(1 - e^{-k_{2,obs} t}) \quad (3)$$

where F is the εA fluorescence as a function of time, C is the fluorescence of the free DNA, Y and Z are the change in fluorescence of the first and second intermediates relative to the free DNA, respectively, E_0 is the starting concentration of AAG and DNA ([AAG] = [DNA]), k_1 is the bimolecular rate constant for binding, $k_{2,obs}$ is the observed unimolecular rate constant for the subsequent flipping step, and t is time. The expression that corresponds to the initial binding step in eq 3 has been previously described (*32*), and the origin of this equation is provided in the Supporting Information.

The fits to eq 3 were excellent in all cases, and the observed rate constants that were obtained were in good agreement with the values of k_1 and $k_{2,obs}$ that were obtained from the binding experiments in which AAG was in excess over DNA.

Pulse−Chase Assay. To measure the rate constant for dissociation of AAG from the εA-containing DNA substrate, pulse−chase experiments were performed. These assays were conducted at 25 °C in the standard buffer, except that the concentration of NaCl was varied and 0.1 mg/mL BSA was added. In 20 μL reaction mixtures, 100 nM fluorescein-labeled TEC DNA was mixed with 200 nM AAG for 20 s. A chase of 20 μM unlabeled TEC DNA was then added. If AAG dissociates from the labeled DNA before the chemical cleavage step and then binds to the unlabeled DNA, less of the reaction will occur during the single-turnover part of the curve as compared to the same experiment without chase. Samples were taken at the specified times and reactions quenched as described above. The samples were run on sequencing gels, and the fraction product was calculated as described above. It was expected that the production of product would follow a simple exponential (eq 1), but under the conditions employed, a very slow steady-state reaction was also observed. Equation 4 accounted for this, in which the burst phase gives the amplitude (A) and an observed rate constant (k_{obs}). The steady-state phase is dependent upon the steady-state rate constant (k_{cat}), the concentration of enzyme (E), and the total concentration of labeled and unlabeled DNA substrate.

$$\text{fraction product} = A(1 - e^{-k_{obs} t}) + (k_{cat}[E]/[DNA]_{total})t \quad (4)$$

According to the two-step binding mechanism described in Scheme 3, two different partitioning equations can be written (*33*). Since all labeled substrate is initially bound, the fraction of product formed is given by the fraction that goes on to react. This is indicated by eq 5

$$A = \frac{k_{max}}{k_{off,obs} + k_{max}} \quad (5)$$

where A is the burst amplitude (the fraction of product cleaved in the burst phase of the experiment), k_{max} is the maximal single-turnover rate constant for formation of product, and $k_{off,obs}$ is the macroscopic rate constant for dissociation from the stable flipped-out complex. This expression can be rearranged to solve for the desired dissociation rate constant (eq 6).

$$k_{off,obs} = \frac{k_{max}}{A} - k_{max} \quad (6)$$

Similarly, for branched pathways, the observed rate constant for the burst phase of the pulse−chase experiment is given by the sum of the rate constants for the competing pathways, formation of product is given by k_{max}, and the macroscopic dissociation of substrate is designated $k_{off,obs}$ (eq 7). Solving for $k_{off,obs}$ gives eq 8.

$$k_{obs} = k_{off,obs} + k_{max} \quad (7)$$

$$k_{off,obs} = k_{obs} - k_{max} \quad (8)$$

Control reactions in which no chase was added provided the single-turnover rate constant, k_{max}, and confirmed that these concentrations of AAG were saturating. From these values, the dissociation rate constant, k_{off}, for dissociation of AAG from εA-DNA was calculated by two different methods (eqs 6 and 8). Both methods gave essentially identical values for $k_{off,obs}$, and we report the average of the results obtained with both methods.

Since the εA-DNA binds in two steps, the observed rate constant for dissociation of substrate ($k_{off,obs}$) could be limited by the unflipping rate (k_{-2}) or dissociation from nonspecific DNA (k_{-1}). According to Scheme 3, and assuming that the flipped-out complex is stable (i.e., $k_2 \gg k_{-2}$), this observed dissociation rate can be expressed in terms of the microscopic rate constants [eq 9 (*33*)]. Stopped-flow fluorescence suggests that dissociation from the initial AAG·DNA complex is rapid ($k_{-1} \sim 30\ s^{-1}$) relative to the forward flipping rate constant ($k_2 = 2.6\ s^{-1}$), and therefore, the observed rate constant for dissociation of substrate from the εA-DNA·AAG complex is approximately equal to the reverse rate constant for flipping.

$$k_{off,obs} = k_{-2}\left(\frac{k_{-1}}{k_{-1} + k_2}\right) \quad (9)$$

The pulse−chase experiment was performed at high and low ionic strengths by varying the concentration of sodium chloride from 50 to 300 mM. It has previously been shown that the rate constant for dissociation of the abasic DNA product increases as the ionic strength is increased, presumably due to the disruption of electrostatic interactions at higher ionic strengths (*13*, *34*).

Steady-State Excision of Hypoxanthine. The maximal rate constant for excision of Hx (k_{cat}) was determined for a 25 bp oligonucleotide of the same sequence as the TEC DNA, but with deoxyinosine in place of the εA. Under multiple-turnover conditions, the rate-limiting step is dissociation of the abasic DNA [$k_{cat} = k_{off}$ for abasic DNA (*34*, *35*)]. The experiments were performed at 25 °C and in the standard buffer that also contained 0.1 mg/mL BSA. In 20 μL reaction mixtures, 2 μM fluorescein-labeled DNA was mixed with 20−50 nM AAG. Aliquots were

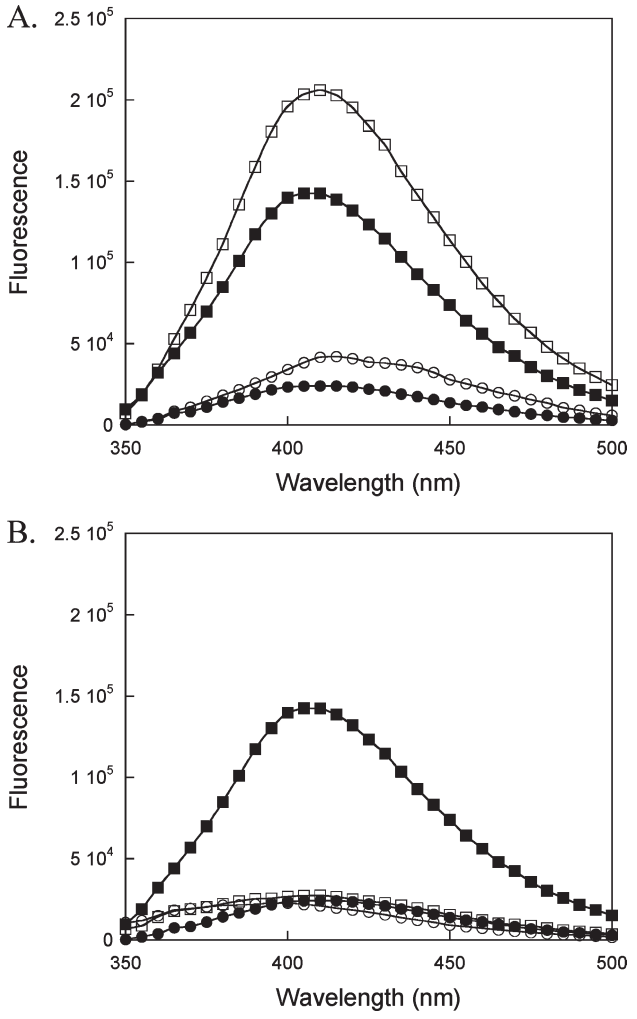

FIGURE 2: Fluorescence of εA-containing DNA in a single strand, in a duplex, and in complex with AAG. Fluorescence emission spectra of 400 nM DNA were collected with excitation at 320 nm, as described in Materials and Methods. (A) Both single-strand (○) and duplex TEC (●) are compared to single-strand (□) and duplex (■) AEA DNA. The εA in both sequences is more fluorescent in the single strand and becomes quenched in the duplex. (B) Fluorescence emission spectra were collected in the presence of a saturating concentration of AAG and compared to the spectra in the absence of AAG. The TEC duplex DNA exhibited very similar fluorescence in the absence (●) or presence (○) of AAG. In contrast, the AEA duplex DNA, which was strongly fluorescent in the absence of protein (■), was strongly quenched in the presence of AAG (□). The spectra were recorded within 1 min of AAG addition (1 μM), during which time negligible excision can occur.

removed at specific times and reactions quenched as described above. These samples were diluted 10-fold into formamide/EDTA buffer, run on sequencing gels, and quantified as described above. The fraction product was converted into the concentration of product ([P] = fraction product × [DNA]). The initial velocity (V_i) was determined from a linear fit to the time-dependent formation of abasic product over the first 15% of the reaction. The value of k_{cat} was calculated by dividing the velocity by the concentration of the enzyme ($k_{cat} = V_i/[E]$).

RESULTS

The Fluorescence of εA Is a Sensitive Reporter of the Lesion Environment. The feasibility of using the intrinsic fluorescence of εA to monitor the individual steps of the AAG-catalyzed reaction was evaluated for two different 25 bp oligonucleotides that each contained a central εA lesion (Scheme 2). Excitation of both single-stranded oligonucleotides at 320 nm gave a broad fluorescence emission peak centered at 410 nm (Figure 2A). The oligonucleotide of sequence TEC gave ~4-fold lower fluorescence than free εA, consistent with quenching of εA fluorescence even in single-stranded DNA. Surprisingly, the oligonucleotide of sequence AEA yielded much higher fluorescence, essentially identical to that of free εA. When a 1.1-fold excess of the appropriate complement was annealed to these sequences, then the fluorescence emission was decreased by a factor of ~1.7-fold for TEC and 1.4-fold for AEA (Table 1). This is consistent with increased quenching due to enhanced base stacking interactions in duplex DNA. Addition of a higher concentration of complement did not further quench the fluorescence (data not shown). It is not clear why these two sequence contexts show such different quenching, but it is possible that the lack of nearby G nucleotides can account for the high fluorescence of the AEA sequence. A previous study of charge transfer between εA and normal bases reported that G is the most efficient quencher of εA, with only modest quenching occurring between εA and C, T, or A bases (*36*). The trivial possibility that the concentration of oligonucleotides was incorrect could be ruled

Table 1: Sequence-Dependent Changes in εA Fluorescence and Rate Constants for Binding and Excision by AAG[a]

	TEC	AEA
ΔF for hybridization[b]	1.7	1.4
ΔF for binding[b]	1.1	5.2
k_{on} (M^{-1} s^{-1})[c]	$(2.1 \pm 0.9) \times 10^8$	$(1.5 \pm 0.4) \times 10^8$
k_{off} (s^{-1})[d]	33 ± 15	48 ± 15
k_{flip} (s^{-1})[e]	2.6 ± 0.1	4.3 ± 0.4
k_{unflip} (s^{-1})[f]	$(2.0 \pm 0.2) \times 10^{-3}$	ND[k]
K_{flip}[g]	1300	ND[k]
k_{chem} (s^{-1})[h]	$(5.7 \pm 0.3) \times 10^{-4}$	$(5.3 \pm 0.2) \times 10^{-4}$
K_d^{ns} (nM)[i]	160	320
$K_d^{εA\text{-}DNA}$ (nM)[j]	0.1	ND[k]

[a]Values are reported at 25 °C in a buffer containing 50 mM NaMES (pH 6.5), 100 mM NaCl, 1 mM EDTA, and 1 mM DTT. [b]εA fluorescence was determined with 400 nM εA-containing DNA and a 3 mm path length cuvette with excitation at 320 nm and emission at 410 nm. The ΔF for hybridization is the ratio of the fluorescence of single-stranded DNA divided by the fluorescence of the double-stranded DNA (Figure 2A). The ΔF for binding to AAG is the ratio of the fluorescence of the double-stranded DNA divided by the fluorescence of the saturated AAG·DNA complex (Figure 2B). [c]The association rate constant (k_{on}) was determined from the data in Figure 7. [d]The dissociation rate constant (k_{off}) was determined from the data in Figure 5. [e]The rate constant for flipping was determined by the stopped-flow method (Figure 7). As discussed in the text, the second phase of the change in εA fluorescence is simply k_{flip}, since k_{unflip} is much slower than k_{flip}. Given the similar rate constants for the two sequences, we assumed that the observed rate constant for the AEA sequence is also the flipping rate constant. [f]The reverse rate constant for flipping [k_{unflip} (Figure 1)] is determined from the macroscopic rate constant for dissociation of the substrate (Figure 8), as described in the text. [g]The equilibrium for nucleotide flipping is defined as the ratio of the forward rate constant for flipping measured by the stopped-flow method and the reverse rate constant for flipping [$K_{flip} = k_2/k_{-2}$ (Scheme 3)]. [h]The rate for the chemical step is simply the rate constant for the single-turnover excision of εA (Figure 3D), since the equilibrium constant for base flipping is highly favorable and the rate constant for flipping is much faster than the hydrolysis step. The values shown are determined from εA fluorescence. For the TEC DNA, a similar value of $(6.8 \pm 0.3) \times 10^{-4}$ s^{-1} was determined from the gel-based assay. [i]The dissociation constant for the nonspecific AAG·DNA complex is given by the ratio of the off and on rates measured by the stopped-flow method ($K_d^{ns} = k_{off}/k_{on}$). [j]The dissociation constant for the specific, flipped-out complex between AAG and εA-DNA is defined by $K_d^{εA\text{-}DNA} = K_d^{ns}/K_{flip}$. [k]Not determined.

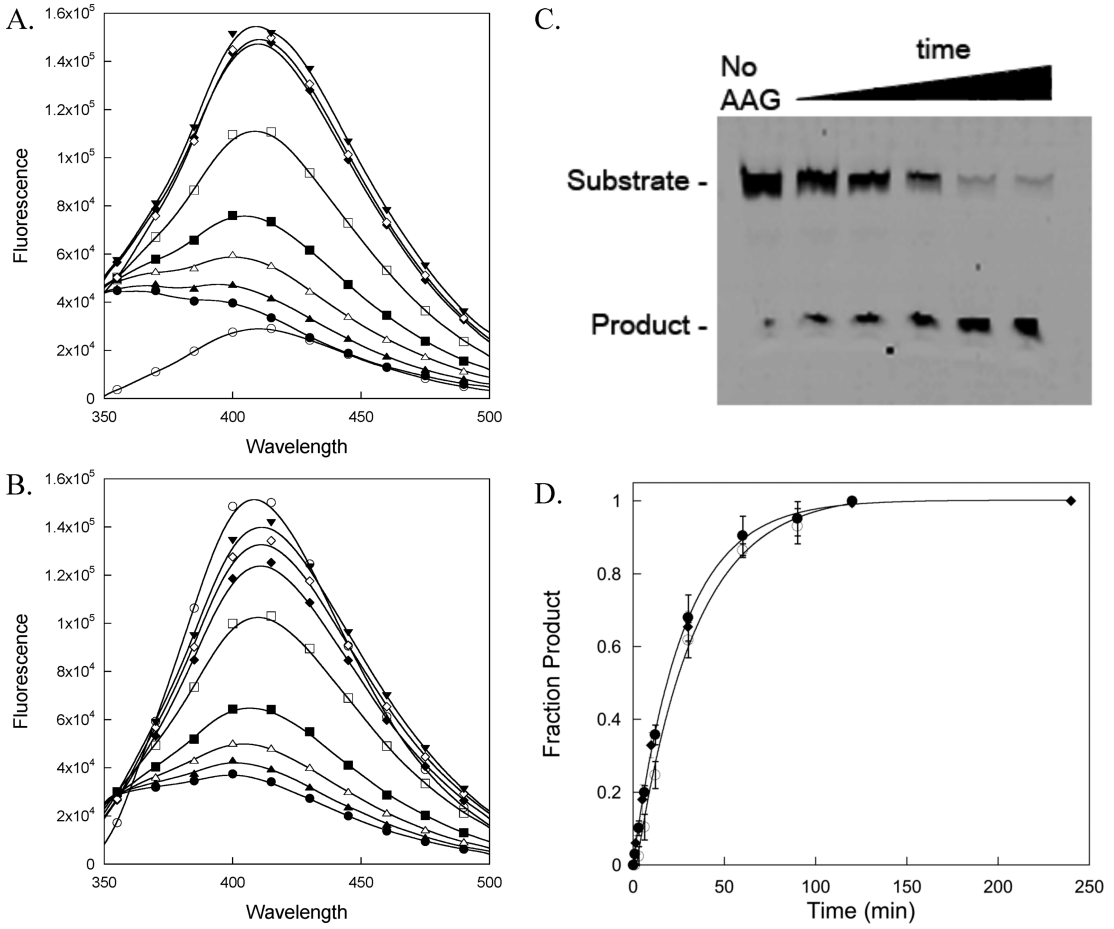

FIGURE 3: Comparison of εA release and N-glycosidic bond cleavage from single-turnover assays. Fluorescence emission spectra monitoring the increase in fluorescence that is observed upon single-turnover excision of εA from (A) TEC and (B) AEA DNA catalyzed by AAG. The spectra for samples containing 400 nM duplex DNA were recorded prior to the addition of protein (○), and within 1 min of the addition of 1.2 μM AAG (●). Additional spectra were collected after 3 (▲), 6 (△), 12 (■), 30 (□), 60 (◆), 90 (◇), and 120 min (▼). Note that the high fluorescence of the AEA substrate is strongly quenched upon binding to AAG. Representative experiments are shown; however, duplicate reactions gave essentially identical results, and the rate of reaction was independent of the concentration of AAG. (C) The gel-based glycosylase assay relies on selective hydroxide-catalyzed cleavage of abasic sites and the different mobility of intact substrate and nicked product in monitoring the formation of the abasic DNA product (see Materials and Methods for details). A representative denaturing polyacrylamide gel shows the separation of the fluorescein-labeled substrate (25-mer) and product (12-mer) and a time course for the formation of the abasic DNA product. The first lane shows a control without enzyme. The small amount of nicked DNA (~4%) results from nonenzymatic ring opening and depurination during synthesis, purification, and the hydroxide heating step. The next five lanes indicate samples taken from a reaction mixture containing 100 nM TEC DNA and 200 nM AAG that were quenched 2−120 min after the initiation of the reaction by the addition of AAG. (D) Quantification of the results from εA release and abasic site formation indicates that both assays are limited by a common step, presumably N-glycosidic bond cleavage. The fraction product was calculated from the εA fluorescence assay for TEC (●) and AEA (○) as well as the gel-based excision assay for TEC (◆), as described in Materials and Methods. The error bars indicate the standard deviation from the mean for two to five independent determinations. The reaction progress curves for TEC monitored by εA fluorescence and abasic site formation are fit by a single exponential (eq 1; $k_{max} = 0.038\ min^{-1}$). The reaction of AEA is slightly slower ($k_{max} = 0.031\ min^{-1}$).

out by measuring the fluorescence of the εA base that is released upon complete hydrolysis by AAG (see below).[2]

Since the AAG-catalyzed excision of εA is relatively slow under these conditions, it was possible to examine the effect of binding of AAG to each oligonucleotide in a conventional fluorometer. The addition of 1 equiv of AAG resulted in a dramatic 5-fold decrease in the fluorescence of the AEA substrate, whereas that of the TEC substrate was only slightly quenched (Figure 2B). Addition of > 1 equiv of AAG had no further effect on either spectrum (data not shown). The two oligonucleotides exhibit almost identical fluorescence emission when they are bound to AAG (Figure 2B). This observation strongly suggests that εA is in a similar environment in both complexes, most likely flipped out of the duplex and bound in the AAG active site. Crystal structures of the AAG·εA-DNA complex indicate potential quenching interactions between the εA lesion and active site tyrosines Y127 and Y159 (*16*). The environment of the protein active site is more strongly quenching than the AEA sequence context, but very similar to that of the TEC sequence context. The strong quenching of both complexes relative to free εA in solution suggested that a continuous fluorescence-based assay could be used to follow the εA excision activity of AAG.

[2]Samples that contained 400 nM of either TEC or AEA duplex (determined using the UV absorbance and the calculated extinction coefficients) gave identical fluorescence emission spectra upon the complete hydrolysis by AAG (Figure 3A,B). This eliminates the trivial possibility that different amounts of DNA were compared. Therefore, we conclude that the AEA sequence has significantly higher fluorescence than the TEC sequence in single-stranded form and when annealed to its complement (Figure 2).

Single-Turnover Glycosylase Activity of AAG Monitored by εA Fluorescence and by Formation of the Abasic DNA Product. Hydrolysis of the N-glycosidic bond by AAG results in the formation of an abasic site and a free base (Figure 1). Early assays of AAG employed alkylated genomic DNA and relied upon directly detecting the released base by HPLC or scintillation counting (*37*, *38*). More commonly, gel-based discontinuous assays are used to detect the formation of a single-strand break (*27*, *29*, *39*). These assays can employ either a fluorescent or radioactive label, and the abasic product is converted into a single-strand nick by hydrolyzing the abasic site at alkaline pH. In contrast, the fluorescent properties of εA provide the opportunity for a continuous glycosylase assay. We directly compared the fluorescence-based assay to the traditional gel-based assay to determine whether εA release is fast or slow and to evaluate the potential of using fluorescence to monitor the glycosylase activity of AAG.

Under single-turnover conditions, with enzyme in excess over the DNA substrate, AAG was incubated with oligonucleotide TEC and fluorescence emission spectra were collected at the indicated intervals (Figure 3A). The εA fluorescence (λ_{max} = 410 nm) increased over time, reaching a maximum value at ~2 h. Under identical conditions, a fluorescein-labeled oligonucleotide of the identical sequence (TEC) was incubated with AAG, and aliquots were quenched in sodium hydroxide and analyzed by denaturing polyacrylamide gel electrophoresis (Figure 3C). The change in fluorescence was converted into the fraction of εA released into solution, and the fraction of abasic product was quantified from the gel; these data were plotted together (Figure 3D; see Materials and Methods for details). The reaction progress curves were readily fit by a single exponential, and the observed rate constants for εA release ($k_{max}^{εA}$ = 0.036 ± 0.002 min^{-1}) and for abasic site formation (k_{max} = 0.038 ± 0.002 min^{-1}) were identical within error. A simultaneous fit to both reaction progress curves gave the same value [k_{max} = 0.038 min^{-1} (Figure 3D)]. Since the detection of the abasic DNA product by sodium hydroxide quench/hydrolysis does not require dissociation of the εA, the observation of the same rate constant for release of εA into solution is most simply consistent with rate-limiting N-glycosidic bond hydrolysis, followed by rapid release of εA.

The single-turnover assay for release of εA was also performed for the AEA DNA under the same conditions that were used for the TEC DNA (Figure 3B). The initial fluorescence of this DNA in the absence of AAG is much higher than for the TEC sequence, but upon the addition of AAG, the fluorescence was strongly quenched. The observed increase in fluorescence was similar in magnitude to that which was observed for the TEC substrate, and a similar single-turnover rate constant was observed [k_{max} = 0.031 ± 0.002 min^{-1} (Figure 3D)].[2] These data indicate that once AAG is bound, it exhibits a very similar efficiency in excising εA from these two different sequence contexts.

Association and Nucleotide Flipping Monitored by Stopped-Flow Fluorescence. The quenching of εA fluorescence observed upon binding of AAG to εA-containing DNA suggested that εA would be a useful reporter for monitoring association of AAG and DNA. Therefore, we performed stopped-flow fluorescence experiments to monitor the time-dependent changes in εA fluorescence. Two phases were observed when excess AAG was mixed with 500 nM TEC DNA, both of which occur well before the base excision step (Figure 4A). In the first 100 ms, there is a transient increase in fluorescence and this is

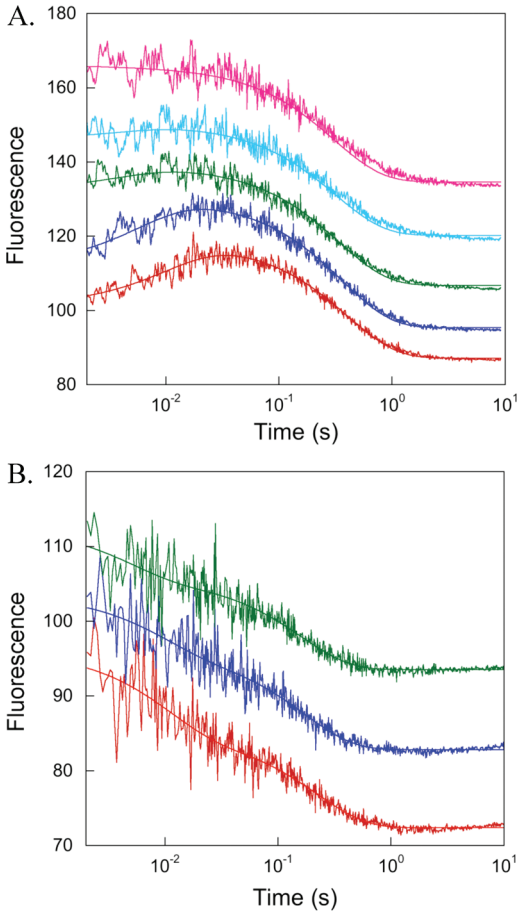

FIGURE 4: Stopped-flow fluorescence measurements of the binding of εA-DNA to AAG with excess protein. Representative data from experiments in which a fixed concentration of DNA was mixed with increasing concentrations of AAG are shown. Samples were excited at 320 nm, and emission was collected with a 360 nm long-pass filter (see Materials and Methods for details). Several individual reactions were monitored at each concentration of AAG, and the traces shown are the averages of all reactions. Since the fluorescence changes were superimposed at the different concentrations of AAG, the traces are offset for the sake of clarity. (A) Binding of 0.5 μM TEC duplex DNA by 0.5 (bottom), 1, 2, 4, and 8 μM (top) AAG. (B) Binding of 0.15 μM AEA duplex DNA by 0.5 (bottom), 1, and 2 μM (top) AAG. The lines indicate the best fits of eq 2 to each binding reaction.

followed by a decrease in fluorescence that is complete within a few seconds of mixing. The fluorescent traces were best fit by a double-exponential equation, indicating a two-step model for DNA binding (Scheme 3). As increasing concentrations of AAG were mixed with a fixed concentration of TEC DNA, the rate of the first phase increased (Figures 4A and 5). However, at concentrations above 1 μM AAG, this initial phase occurred in the mixing time of the stopped flow. The dependence of the first phase of the fluorescence change upon the concentration of reactants indicates that a bimolecular event is being monitored. It should be noted that the fit of the two concentrations of AAG with the TEC substrate in Figure 5 is tenuous; however, it was possible to measure binding over a wider concentration range for the more highly fluorescent AEA DNA.

Since initial binding is expected to be away from the site of damage, and the bimolecular step gives a detectable change in fluorescence, we interpret this behavior as reflecting a rate-limiting binding step with no change in fluorescence, followed by a rapid sliding step that results in the formation of a complex with a detectable change in fluorescence. We infer that

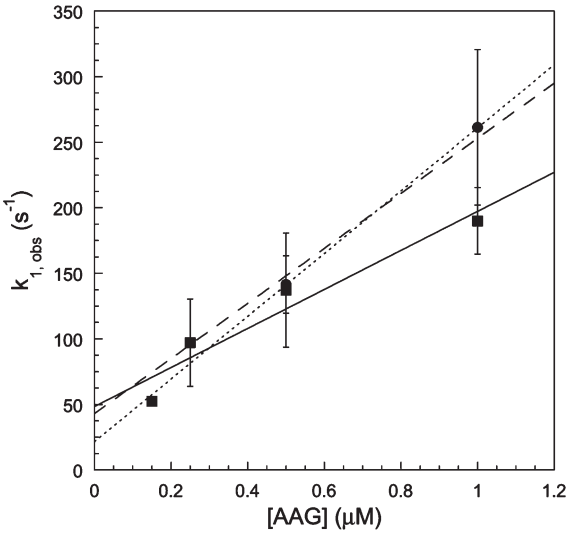

FIGURE 5: Determination of the forward and reverse rate constants for the initial binding of AAG to εA-DNA. The observed rate constant for DNA binding ($k_{1,obs}$) is from the first phase of the binding reactions shown in Figure 4. The average and standard deviations are shown for two to four determinations. The dissociation rate constant for the initial AAG·DNA complex can be determined from the *y*-intercept of this plot [$k_{1,obs} = k_{-1} + k_1$[AAG] (Scheme 3)]. For AEA DNA (■), the best linear fit (—) gives an intercept of 48 s^{-1} (k_{-1}) and a slope of 1.5×10^8 M^{-1} s^{-1} (k_1). This second-order rate constant is identical to the value determined from equimolar binding experiments (Table 1 and Figure 7). For TEC DNA (●), only two concentrations of protein gave reliable data due to the weak fluorescence and more rapid binding. A linear fit (···) of the two data points that were obtained gives an intercept of 22 s^{-1} and a slope of 2.4×10^8 M^{-1} s^{-1}. By forcing the slope of the line to be 2.1×10^8 M^{-1} s^{-1} (---), the value that was independently determined from equimolar binding reactions (Table 1 and Figure 7), we obtained an intercept of 43 s^{-1}. We take the average (33 ± 15 s^{-1}) as a rough estimate for the k_{-1} value for this substrate.

the scanning step is too fast to be directly observed in our experiments (Figure 1), with a lower limit of 250 s^{-1} indicated by the data in Figure 5. The increased fluorescence of this early intermediate is likely to reflect partial unstacking of the εA lesion during the initial damage recognition by AAG. The second phase of the binding reaction was insensitive to the concentration of AAG, and we interpret this to be the flipping of the εA lesion into the AAG active site, where it is strongly quenched. For the TEC substrate, this AAG-bound complex happens to have a fluorescence very similar to that of the free DNA duplex in solution (Figure 2B).

We performed analogous stopped-flow binding experiments with the AEA substrate (Figure 4B). Binding of AAG to this sequence appears to be superficially different, without a transient increase in fluorescence, but is also best explained by a two-step binding mechanism. For this substrate, the fluorescence is initially high in the free DNA, is partially quenched in the first intermediate, and is more strongly quenched in the fully flipped complex. These traces could not be fit well by a single exponential (data not shown) but were well fit by a double exponential (Figure 4B). As the concentration of AAG was increased at a fixed concentration of DNA, the rate for the first exponential was proportional to the amount of AAG, and the second phase was not (Figures 4 and 5 and data not shown). The fits to the second phase of the reaction were excellent in all cases, but the fits to the first phase were more variable due to the very fast binding. As the fluorescence of εA is relatively weak, it was not possible to use significantly lower concentrations of DNA that would have

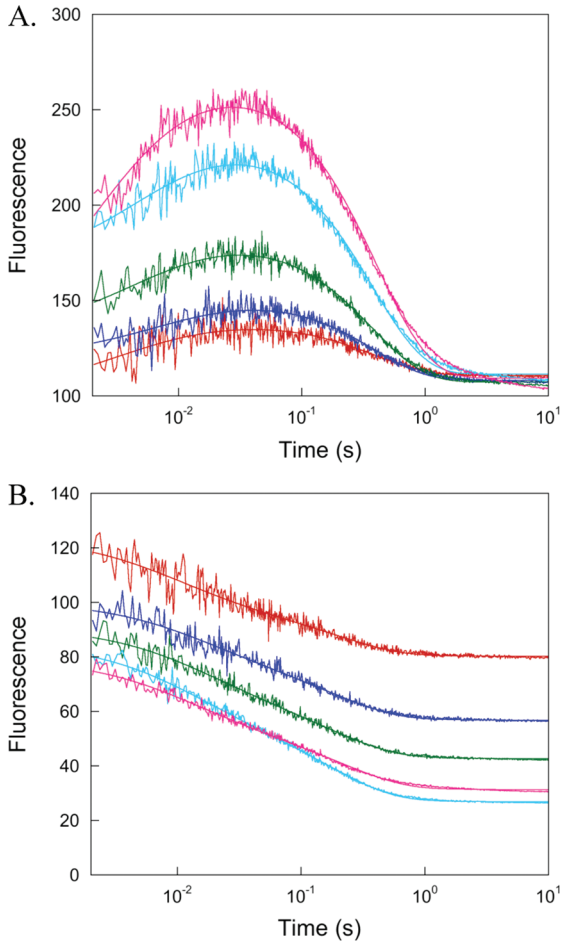

FIGURE 6: Kinetics of DNA binding and nucleotide flipping, determined by stopped-flow fluorescence at equimolar concentrations of AAG and DNA. AAG was rapidly mixed with an equimolar solution of TEC (A) or AEA (B) DNA to yield final concentrations after mixing from 0.15 (bottom) to 1.5 μM (top). Each trace is the average of three independent binding reactions, and the lines indicate the best fits of eq 3. For the TEC substrate, the raw data are plotted, indicating the increased signal observed at higher concentrations of DNA; however, for the AEA substrate, the larger fluorescence change required that the gain be adjusted between different concentrations of DNA, and therefore, the individual traces are arbitrarily offset.

allowed more accurate determination of the association and dissociation rate constants of this fast binding reaction.

Therefore, the stopped-flow experiments were repeated with equimolar amounts of enzyme and substrate, with concentrations ranging from 0.15 to 1.5 μM (Figure 6). This causes the binding reaction to slow as free ligand is consumed, allowing a time-dependent change in fluorescence to be observed even at high initial concentrations. Similar experiments have been used to study binding reactions of equimolar protein fragments (*40*, *41*). Since the unimolecular flipping step also gives an observed fluorescence change, a second exponential term is also required (eq 3). The fitting of this equation to the data in Figure 6 gave similar association rate constants of ~2×10^8 M^{-1} s^{-1} for both sequences (Figure 7A and Table 1). Experiments conducted over a 10-fold concentration range gave the same rate constant. This better-defined value for the association rate constant [k_1 (Scheme 3)] was used to fit the data from the concentration dependence of AAG when protein was in excess and provide an estimate of the dissociation rate constant [$k_{-1} \approx 30$ s^{-1} (Figure 5 and Table 1)].

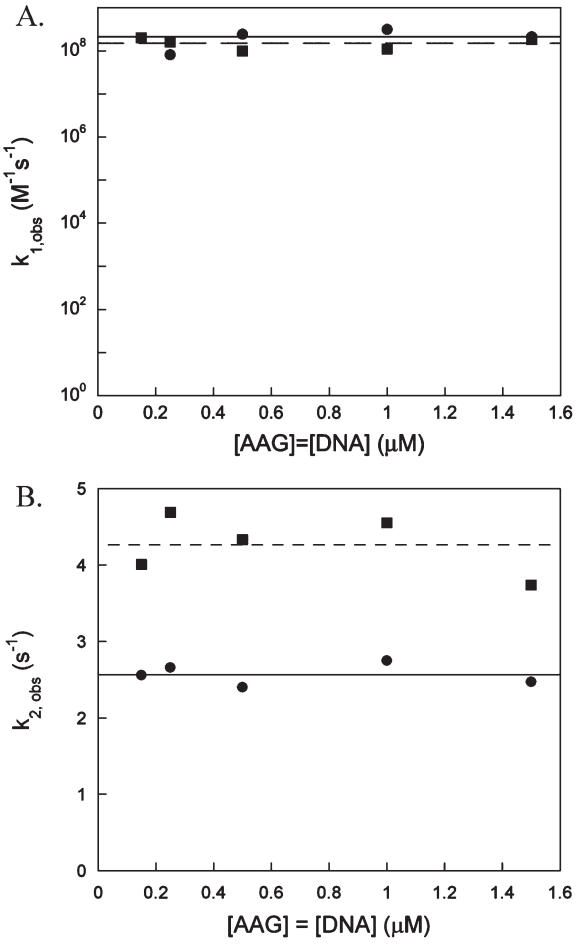

FIGURE 7: Rate constants for binding and nucleotide flipping by AAG in two different sequence contexts. The observed rate constants for TEC DNA (●, solid line) and AEA DNA (■, dashed line) were taken from the fits of eq 3 to the data for equimolar binding reactions (Figure 6). (A) The observed bimolecular rate constant for the initial binding of AAG to DNA is very similar for both substrates [$\sim 2 \times 10^8$ M^{-1} s^{-1} (Table 1)]. According to the simple two-step binding mechanism depicted in Scheme 3, this observed rate constant is simply k_1, the microscopic rate constant for binding. (B) The observed rate constant for the second step is independent of concentration and yields an average value of 4.3 s^{-1} for the AEA sequence context compared to a value of 2.6 s^{-1} for the TEC sequence context. According to Scheme 3, this observed rate constant is the sum of the forward and reverse rate constants for flipping ($k_{2,obs} = k_2 + k_{-2}$). Additional experiments described below indicate that the equilibrium constant for flipping is highly favorable ($k_2 \gg k_{-2}$), and therefore, the observed rate constant for flipping is simply the forward rate constant for flipping (see the text for additional discussion).

The second phase of the binding reaction followed a single exponential, and the same rate constant was observed across the concentration range tested (Figure 7B). The observed rate constant for flipping is an approach to equilibrium and therefore is the sum of the forward and reverse rate constants for flipping [$k_{2,obs} = k_2 + k_{-2}$ (Scheme 3)]. Below we describe a pulse−chase experiment that resolves this ambiguity by establishing that the reverse rate constant for flipping (k_{-2}) is much slower than the rate constant measured by the stopped-flow fluorescence, such that the observed rate constant is simply the forward rate constant for flipping ($k_{2,obs} = k_{flip}$). The nucleotide flipping step (k_{flip}) is significantly faster for the AEA sequence (4.3 ± 0.4 s^{-1}) than for the TEC sequence (2.6 ± 0.1 s^{-1}). The difference in the rates of flipping in two different sequence contexts may reflect subtle differences in how AAG engages these different DNA molecules or sequence-dependent changes in the intrinsic motions of DNA. Regardless of the origin of the differences between the two sequence contexts that were examined, these data establish that the flipping step is much faster than the N-glycosidic bond hydrolysis step (Table 1).

A Pulse−Chase Assay To Determine the Macroscopic Rate of Substrate Dissociation. To gain further insight into the two-step binding mechanism of AAG, we also examined the dissociation of substrate from AAG by a pulse−chase assay (*30*, *33*). In this experiment, fluorescein-labeled TEC substrate was briefly incubated with AAG (t_1 = 20 s) to give it time to bind and then was chased with a 100-fold excess of TEC substrate lacking the fluorescein label (Figure 8A). Samples were taken over the normal single-turnover time course to evaluate the partitioning of a bound E·S complex between N-glycosidic bond hydrolysis and dissociation. Figure 8B shows the εA excision reaction in the presence and absence of chase. The addition of chase caused a decrease in the fraction of substrate hydrolyzed and an increase in the observed rate constant, as expected if the forward rate constant for reaction is similar to the rate constant for dissociation (see Materials and Methods for details). Under these conditions (I = 120 mM), the macroscopic rate constant for dissociation is 0.12 ± 0.02 min^{-1} (Table 1). Since the equilibrium for bound εA-DNA lies toward the fully flipped-out complex, either k_{-1} or k_{-2} could in principle limit the observed rate constant for dissociation. However, the rapidly reversible initial binding step exhibits a much faster rate constant [$k_{-1} \sim 30$ s^{-1} (Figure 5)]. Therefore, the observed rate constant for the dissociation of the substrate that was measured by the pulse−chase assay is simply the unflipping rate constant [k_{-2} (Scheme 3; see Materials and Methods for additional details)].

It has previously been observed that the rate of dissociation of AAG from its abasic DNA product is extremely sensitive to the ionic strength, with a 25-fold increase in the rate of dissociation between ionic strengths of 40 and 120 mM (*34*). This effect of ionic strength is presumably due to electrostatic interactions between the positively charged protein and the negatively charged DNA that become weaker at higher ionic strength. To evaluate whether the unflipping rate constant or the DNA dissociation rate constant is rate-limiting, we varied the ionic strength with the expectation that the dissociation step should exhibit a large ionic strength effect. The results of pulse−chase experiments conducted at ionic strengths of 70, 120, and 320 mM are shown in Figure 8C. The pulse−chase experiment revealed a small decrease in amplitude and concomitant increase in the observed rate constant as the ionic strength is increased. Control reactions established that the single-turnover rate constant in the absence of chase is independent of ionic strength under these conditions (data not shown), consistent with previous results (*13*, *34*). Therefore, the ~4-fold change in the observed substrate dissociation rate constant between 70 and 320 mM is further evidence that k_{-2} and not k_{-1} is rate-limiting for dissociation of εA-DNA. This moderate sensitivity to ionic strength indicates either a small effect of ionic strength on the flipping step or a small contribution from the rate constant for dissociation from nonspecific DNA.

Rate Constant for Dissociation of the Abasic DNA Product. We measured the rate of dissociation of the abasic DNA product to compare it to the rate of εA product release. The steady-state reaction of AAG with TEC substrate gave a k_{cat} value that is essentially identical to the single-turnover rate constant under these reaction conditions (data not shown), suggesting that

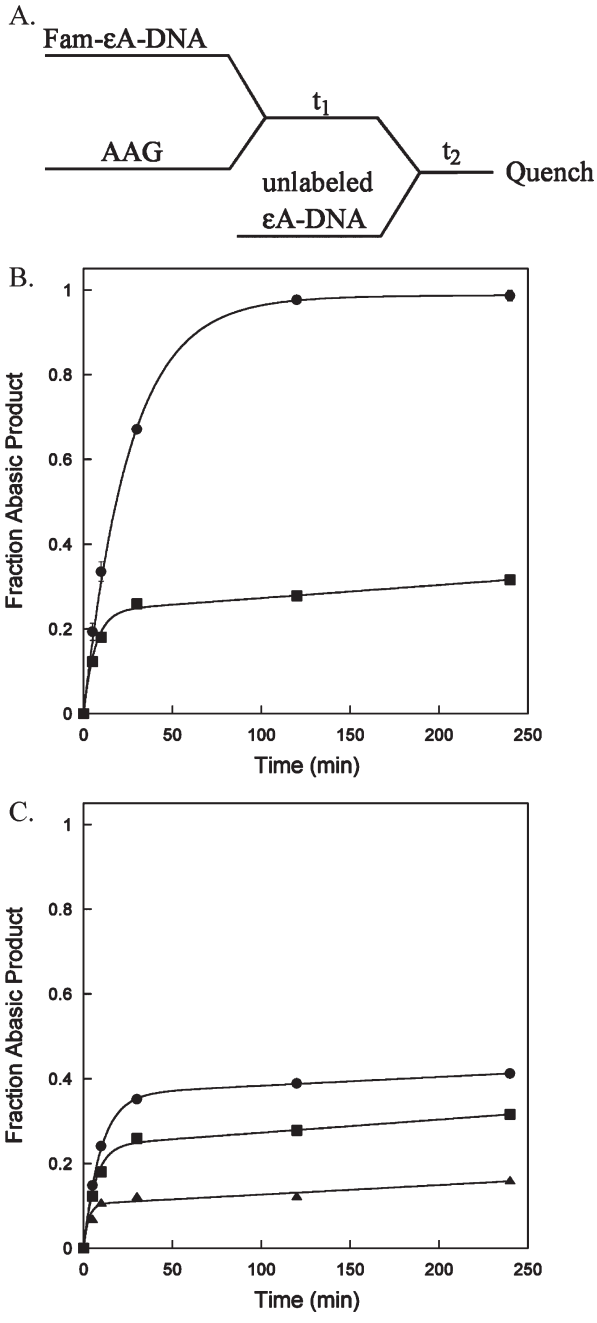

FIGURE 8: Pulse−chase experiment for measuring the macroscopic dissociation rates for εA-containing DNA substrate. (A) Experimental design. Fluorescein (fam)-labeled DNA (100 nM TEC) was mixed with excess AAG (200 nM) for 20 s (incubation time, t_1), and then 20 μM unlabeled TEC DNA was added as a chase. The reactions were quenched at the indicated time points (t_2), and the fraction of abasic DNA product was determined by alkaline hydrolysis and gel electrophoresis (see Materials and Methods for additional details). (B) Single-turnover excision of εA from TEC DNA by AAG in the absence (●) or presence (■) of chase under the standard reaction conditions. In the absence of chase, the line indicates the best fit to a single exponential (eq 1). In the presence of chase, the line indicates the best fit of an exponential burst followed by a slow steady-state reaction (eq 4). This gives a macroscopic dissociation rate constant of 0.12 ± 0.01 min^{-1}. (C) Comparison of pulse−chase experiments performed at different sodium chloride concentrations. The data from experiments at ionic strengths of (●) 70, (■) 120, and (▲) 320 mM were fit by eq 4 (lines). Analysis of the observed rate constant and the end point gave essentially identical macroscopic rate constants, and the average and standard deviation of duplicate reactions determined by both methods yielded macroscopic dissociation rate constants of 0.08 ± 0.005, 0.12 ± 0.01, and 0.35 ± 0.05 min^{-1} for ionic strengths of 70, 120, and 320 mM, respectively.

Scheme 4

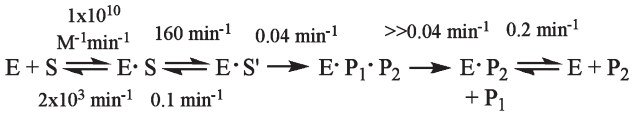

the very slow rate of hydrolysis of the N-glycosidic bond is rate-limiting for multiple-turnover excision of εA at high ionic strengths. Since AAG shows much faster rates of excision of Hx from inosine lesions, we measured the k_{cat} value for multiple turnovers on an inosine-containing substrate. It has previously been shown that AAG exhibits burst kinetics for the excision of Hx and that the steady-state rate constant, k_{cat}, reflects the rate of dissociation of the abasic DNA product (*34*). We determined that the rate constant for the dissociation of abasic DNA is 0.24 min^{-1} under these reaction conditions, ~6-fold faster than the rate constant for N-glycosidic bond cleavage (Scheme 4; see the Supporting Information). This is only slightly faster than the observed rate constant for dissociation of the εA substrate ($k_{off,obs}$ = 0.12 min^{-1}), suggesting that the abasic DNA product is also likely to be stably bound in an extrahelical conformation.

DISCUSSION

Minimal Kinetic and Thermodynamic Mechanism for Excision of εA. We have used the intrinsic fluorescence of the εA lesion to establish the kinetic mechanism for the AAG-catalyzed recognition and excision of this alkylated base. The fluorescence of εA is highly sensitive to the local environment of the lesion, and it proved to be a sensitive reporter of three distinct steps in the AAG-catalyzed reaction: initial lesion recognition, nucleotide flipping, and εA product release. The rate constants that were determined from changes in εA fluorescence are in excellent agreement with the rate constants measured by the traditional glycosylase assay that detects the abasic DNA product, indicating that εA release is fast and that fluorescence provides a useful assay of AAG activity.

The kinetic mechanism for recognition and excision of εA is depicted for the TEC sequence in Scheme 4. Initial binding is near the diffusion-limited rate and is rapidly reversible. Given that a detectable change in εA fluorescence occurs as a bimolecular reaction, we cannot distinguish between the possibilities that initial binding by AAG occurs solely at the εA lesion or that AAG binds at another site but rapidly transfers to the εA lesion. We favor the latter model, since it is known that AAG can use nonspecific DNA binding interactions to translocate between sites (*13*). Since these data require the scanning step(s) to be very rapid [k_{scan} (Figure 1)], this step is not shown in Scheme 4. This initial recognition complex is rapidly reversible, with a dissociation rate constant of ~1800 min^{-1}. This indicates a relatively weak complex for initial nonspecific DNA binding, and we calculate a dissociation constant of ~150 nM from these data [K_d^{ns} (Table 1)]. Occasionally, AAG catalyzes full nucleotide flipping with a rate constant of ~160 min^{-1}. The extrahelical complex is highly stable, with a calculated equilibrium constant of ~1300 for the flipping step, and this tight binding decreases the dissociation constant for binding of AAG to an εA lesion by several orders of magnitude to approximately 100 pM (Table 1). This exceptionally tight binding to the εA site is consistent with previous reports of subnanomolar binding by AAG under different experimental conditions (*2*, *42*). The crystal structure of AAG bound to εA reveals a snug fit of the εA lesion into the

Table 2: Comparison of Nucleotide Flipping by DNA Repair Glycosylases

enzyme	superfamily[a]	substrate	k_{flip} (s^{-1})	k_{unflip} (s^{-1})	K_{flip}	k_{chem} (s^{-1})[b]	ref
			Narrow Substrate Range				
UDG	UDG	2′-fluoroU·G	1260	38	33	N/A[c]	*17*
		U·A	1100	370	3	58	*18*
		U (AUA)[d]	670	16	41	38	*19*
		U (GUC)[d]	48	12	4	ND[e]	*19*
T4 Pdg	HhH	D·2AP[f]	≥300	ND[e]	≥10	N/A[c]	*20*
Ogg1	HhH	8-oxo-G·C	13	1	10	0.07	*21*
			Broad Substrate Range				
Fpg	Fpg	8-oxo-G·C	12	12	1	0.16	*22*
AAG	AAG	εA·T	3	0.002	1300	0.0006	this study

[a]HhH, helix−hairpin−helix superfamily. UDG (uracil DNA glycosylase), Fpg (formamidopyrimidine DNA glycosylase), and AAG are the founding members of distinct enzyme superfamilies. T4 Pdg, pyrimidine dimer DNA glycosylase from phage T4, and Ogg1, human 8-oxoguanine DNA glycosylase. [b]k_{chem} is the rate constant for the first chemical step, hydrolysis of the N-glycosidic bond. [c]Not applicable. [d]Rate constants for binding of UDG to single-stranded DNA with two different sequence contexts. It should be noted that a very different process of nucleotide selection is expected in single-strand and duplex DNA, but the values are included here because they are remarkably similar to the values that were independently measured for the enzyme binding to duplex DNA. [e]Not determined. [f]The D·2AP (tetrahydrofuran·2-aminopurine) pair mimics an abasic site product.

AAG pocket where it accepts a hydrogen bond from the backbone amide of His136 (*16*). This interaction with His136 can also account for the discrimination against normal adenosine nucleotides (*2*, *16*). Tight binding of the damaged nucleotide by AAG could protect it from DNA-templated activities such as transcription and replication.

Despite the rapid and highly favorable flipping of the εA lesion, AAG is limited by a very slow rate of N-glycosidic bond cleavage, such that the specific recognition complex is only partially committed to base excision. The rate of release of εA, measured by the increased fluorescence of the free base, is much faster than the rate of N-glycosidic bond cleavage measured by formation of the abasic DNA product. At 25 °C, this rate constant for N-glycosidic bond cleavage is 0.04 min^{-1}, 5-fold slower than that observed at 37 °C (*2*). Under these conditions, base excision is also slower than release of the abasic DNA product, such that no burst is observed (Table 1 and data not shown). Since N-glycosidic bond cleavage for inosine is much faster than for εA, the slow release of the abasic DNA product is rate-limiting for the multiple-turnover reaction of AAG with inosine and other rapidly hydrolyzed lesions (*34*). Rate-limiting release of the abasic DNA product provides the opportunity for coordination of the steps of the BER pathway. It has previously been shown that the slow rate of dissociation of AAG from its abasic DNA product can be stimulated by APE1, the enzyme that acts next in the base excision repair pathway (*34*, *35*, *43*).

Recognition of εA in a Poly(A) Tract. Earlier studies had investigated the AAG-catalyzed excision of εA from different sequence contexts. One study reported that the excision of εA by AAG is sensitive to the sequence context and that an εA lesion in the center of a poly(A) tract is a particularly poor substrate for AAG (*27*). In contrast, a later report examined a number of similar sequence contexts and found that there did not appear to be but significant effects of sequence context on the excision of εA (*26*). However, Hx-containing substrates show large sequence context effects hinting at a fundamental difference between the recognition of εA and Hx (*25*, *26*, *43*, *44*). In this study, we performed a more thorough kinetic characterization to compare the recognition of εA in the poly(A) tract (AEA) and in a heterogeneous sequence (TEC).

Overall, the steps of εA recognition and excision by AAG are very similar for the two DNA substrates (Table 1). The rate constants for DNA binding and excision are identical within error, but the observed rate constant for flipping is ∼1.7-fold higher for the poly(A) tract sequence. Although this is a small change, the rate constant for flipping is independent of DNA and enzyme concentration and is sufficiently well-defined by the stopped-flow data to indicate a real difference. This difference in rate could be due to changes in either the structure or the dynamics of different DNA sequences. Nevertheless, since nucleotide flipping is rapid and highly favorable, the difference in flipping rate does not translate into a significant difference in the rate of excision of εA from these two sequences. The minimal kinetic and thermodynamic framework (Scheme 3) provides a molecular explanation for why AAG does not exhibit strong sequence-dependent differences in the rates of excision of εA but does show strong effects for other lesions. By extension, it is very likely that other lesions that are recognized by AAG, such as the deaminated base lesion Hx, are not stably flipped, and thus, changes in stacking interactions have a larger effect on the flipping equilibrium and on the observed rates of excision (*2*, *25*).

Comparison of AAG to Other Glycosylases. There are several distinct structural and evolutionary families of DNA repair glycosylases (*45*, *46*). These enzymes differ in their chemical mechanisms and in the identity of the lesions that they recognize, but nonetheless, all recognize damaged bases and catalyze the cleavage of the N-glycosidic bond (*47*, *48*). The observation that all of these enzymes that recognize nucleotides in duplex DNA catalyze nucleotide flipping attests to the requirement of the enzyme to gain access to the N-glycosidic bond that is occluded in duplex DNA (*26*). Fluorescence methods have been used to study the DNA binding and nucleotide flipping steps for a few of these enzymes, and the results from the literature are summarized in Table 2. Since each of these enzymes belongs to a different superfamily and therefore evolved independently, it is interesting to consider whether there are common functional constraints that have dictated the kinetic mechanism of the enzyme (*46*, *49*, *50*). One crude classification that can be used is whether the enzyme exhibits a narrow substrate range (recognizing one or a few structurally related lesions) or whether

it exhibits a broad substrate range (recognizing a variety of structurally diverse lesions). The rate constant for flipping varies across 2 orders of magnitude from 3 to $>1000\ s^{-1}$. With these limited data, it seems that the enzymes with a narrow substrate range exhibit faster flipping rates than those with a broader substrate range. This could be related to the difficulty of optimizing the rate of flipping of distinct lesions by the enzymes with a broad substrate range, or it could simply reflect the slow rate of N-glycosidic bond cleavage since the flipping step is still much faster than the hydrolysis step. Indeed, the nucleotide flipping step is much faster than the N-glycosidic bond cleavage step for all of these enzymes (Table 2).

The equilibrium constant for flipping is close to unity for formamidopyrimidine DNA glycosylase (Fpg), the only enzyme with a broad substrate range that has been previously characterized. It makes sense that an enzyme that can accommodate structurally diverse lesions might not be able to hold all lesions tightly. In contrast, the enzymes that recognize a narrow range of substrates all exhibit favorable equilibrium constants for flipping of ≥ 10. Interestingly, AAG has an exceptionally broad range of substrates and yet also has the most highly favorable equilibrium constant for flipping that has been measured. Biochemical evidence suggests that εA is unique among the well-characterized AAG substrates, because other lesions such as 7-methylguanosine and inosine appear to have unfavorable equilibrium constants for flipping by AAG (*2*, *25*).

Implications of Multistage Recognition for the Biological Specificity of AAG. The findings presented above have several implications for the initiation of base excision repair by AAG. The most obvious is that the kinetic mechanism is optimized for specificity rather than speed. The vast excess of undamaged nucleotides in DNA provides a challenge to an enzyme that must recognize a broad range of structurally distinct substrates. Two-step binding is rapid and readily reversible at each step, which provides multiple opportunities for discrimination between damaged and undamaged bases. The multiplicative effect of multistage recognition allows even small differences between normal and damaged bases to be magnified to achieve the specificity that is required to recognize rare lesions that can occur throughout the genome.

Once the lesion is flipped, rate-limiting N-glycosidic bond cleavage allows for additional discrimination between damaged and undamaged nucleotides. Pyrimidines are selected against by the catalytic mechanism, which is optimized for purine nucleotides, and A and G are selected against by steric clashes with their exocyclic amino groups (*2*, *16*, *29*, *51*). Since alkylated nucleotides that bear positive charge are activated for N-glycosidic bond cleavage, some alkylated purines are removed at biologically relevant levels despite the relatively poor rate enhancement (*52*, *53*).

We propose that the highly favorable equilibrium constant for the flipping of εA by AAG is the exception that proves the rule. The opposing base effects that have previously been noted strongly suggest that the equilibrium constant for flipping methylated and deaminated purines is unfavorable (*2*, *25*). In spite of this unfavorable equilibrium, many of these other lesions are excised by AAG more rapidly than the εA lesion is excised. The favorable equilibrium constant for εA helps to compensate for the very slow rate of base excision. If εA is not repaired, it is highly mutagenic, and therefore, it must be removed from the genome. However, human cells have a relatively long cell cycle, and this provides a wide window of time during which repair can be performed prior to DNA replication. Therefore, DNA repair enzymes can afford to sacrifice speed (overall rate of reaction) for increased selectivity (ability to recognize subtle perturbations in the chemical structure of DNA). AAG is able to effectively locate rare sites of damage that are hidden in the sea of undamaged DNA by employing multiple DNA binding steps that are rapidly reversible and each provide specificity toward DNA damage.

ACKNOWLEDGMENT

We thank Dave Ballou and Bruce Palfey for advice and for the use of their stopped-flow instruments, Carol Fierke for the suggestion of studying binding at equimolar concentrations, and Suzanne Admiraal, Alex Ninfa, and members of the O'Brien lab for helpful discussions and comments on the manuscript. We also thank an anonymous reviewer for careful critique of the kinetics.

SUPPORTING INFORMATION AVAILABLE

Fluorescence excitation spectra of the εA-containing DNA, representative single-turnover data showing that a saturating concentration of AAG was used to measure the single-turnover reaction, and representative multiple-turnover data that were used to determine k_{cat} for the excision of Hx. This material is available free of charge via the Internet at http://pubs.acs.org.

REFERENCES

1. Robertson, A. B., Klungland, A., Rognes, T., and Leiros, I. (2009) DNA repair in mammalian cells: Base excision repair: The long and short of it. *Cell. Mol. Life Sci. 66*, 981–993.
2. O'Brien, P. J., and Ellenberger, T. (2004) Dissecting the broad substrate specificity of human 3-methyladenine-DNA glycosylase. *J. Biol. Chem. 279*, 9750–9757.
3. Hitchcock, T. M., Dong, L., Connor, E. E., Meira, L. B., Samson, L. D., Wyatt, M. D., and Cao, W. (2004) Oxanine DNA glycosylase activity from mammalian alkyladenine glycosylase. *J. Biol. Chem. 279*, 38177–38183.
4. Gros, L., Ishchenko, A. A., and Saparbaev, M. (2003) Enzymology of repair of etheno-adducts. *Mutat. Res. 531*, 219–229.
5. Speina, E., Zielinska, M., Barbin, A., Gackowski, D., Kowalewski, J., Graziewicz, M. A., Siedlecki, J. A., Olinski, R., and Tudek, B. (2003) Decreased repair activities of 1,N(6)-ethenoadenine and 3,N(4)-ethenocytosine in lung adenocarcinoma patients. *Cancer Res. 63*, 4351–4357.
6. Pandya, G. A., and Moriya, M. (1996) 1,N6-Ethenodeoxyadenosine, a DNA adduct highly mutagenic in mammalian cells. *Biochemistry 35*, 11487–11492.
7. Levine, R. L., Yang, I. Y., Hossain, M., Pandya, G. A., Grollman, A. P., and Moriya, M. (2000) Mutagenesis induced by a single 1,N6-ethenodeoxyadenosine adduct in human cells. *Cancer Res. 60*, 4098–4104.
8. Ringvoll, J., Moen, M. N., Nordstrand, L. M., Meira, L. B., Pang, B., Bekkelund, A., Dedon, P. C., Bjelland, S., Samson, L. D., Falnes, P. O., and Klungland, A. (2008) AlkB homologue 2-mediated repair of ethenoadenine lesions in mammalian DNA. *Cancer Res. 68*, 4142–4149.
9. Elder, R. H., Jansen, J. G., Weeks, R. J., Willington, M. A., Deans, B., Watson, A. J., Mynett, K. J., Bailey, J. A., Cooper, D. P., Rafferty, J. A., Heeran, M. C., Wijnhoven, S. W., van Zeeland, A. A., and Margison, G. P. (1998) Alkylpurine-DNA-N-glycosylase knockout mice show increased susceptibility to induction of mutations by methyl methanesulfonate. *Mol. Cell. Biol. 18*, 5828–5837.
10. Engelward, B. P., Weeda, G., Wyatt, M. D., Broekhof, J. L., de Wit, J., Donker, I., Allan, J. M., Gold, B., Hoeijmakers, J. H., and Samson, L. D. (1997) Base excision repair deficient mice lacking the Aag alkyladenine DNA glycosylase. *Proc. Natl. Acad. Sci. U.S.A. 94*, 13087–13092.
11. Kisby, G. E., Olivas, A., Park, T., Churchwell, M., Doerge, D., Samson, L. D., Gerson, S. L., and Turker, M. S. (2009) DNA repair modulates the vulnerability of the developing brain to alkylating agents. *DNA Repair 8*, 400–412.
12. Meira, L. B., Moroski-Erkul, C. A., Green, S. L., Calvo, J. A., Bronson, R. T., Shah, D., and Samson, L. D. (2009) AAG-initiated base excision repair drives alkylation-induced retinal degeneration in mice. *Proc. Natl. Acad. Sci. U.S.A. 106*, 888–893.

13. Hedglin, M., and O'Brien, P. J. (2008) Human alkyladenine DNA glycosylase employs a processive search for DNA damage. *Biochemistry 47*, 11434–11445.
14. Roberts, R. J., and Cheng, X. (1998) Base flipping. *Annu. Rev. Biochem. 67*, 181–198.
15. Lau, A. Y., Scharer, O. D., Samson, L., Verdine, G. L., and Ellenberger, T. (1998) Crystal structure of a human alkylbase-DNA repair enzyme complexed to DNA: Mechanisms for nucleotide flipping and base excision. *Cell 95*, 249–258.
16. Lau, A. Y., Wyatt, M. D., Glassner, B. J., Samson, L. D., and Ellenberger, T. (2000) Molecular basis for discriminating between normal and damaged bases by the human alkyladenine glycosylase, AAG. *Proc. Natl. Acad. Sci. U.S.A. 97*, 13573–13578.
17. Stivers, J. T., Pankiewicz, K. W., and Watanabe, K. A. (1999) Kinetic mechanism of damage site recognition and uracil flipping by *Escherichia coli* uracil DNA glycosylase. *Biochemistry 38*, 952–963.
18. Wong, I., Lundquist, A. J., Bernards, A. S., and Mosbaugh, D. W. (2002) Presteady-state analysis of a single catalytic turnover by *Escherichia coli* uracil-DNA glycosylase reveals a "pinch-pull-push" mechanism. *J. Biol. Chem. 277*, 19424–19432.
19. Bellamy, S. R., Krusong, K., and Baldwin, G. S. (2007) A rapid reaction analysis of uracil DNA glycosylase indicates an active mechanism of base flipping. *Nucleic Acids Res. 35*, 1478–1487.
20. Walker, R. K., McCullough, A. K., and Lloyd, R. S. (2006) Uncoupling of nucleotide flipping and DNA bending by the t4 pyrimidine dimer DNA glycosylase. *Biochemistry 45*, 14192–14200.
21. Kuznetsov, N. A., Koval, V. V., Zharkov, D. O., Vorobjev, Y. N., Nevinsky, G. A., Douglas, K. T., and Fedorova, O. S. (2007) Pre-steady-state kinetic study of substrate specificity of *Escherichia coli* formamidopyrimidine-DNA glycosylase. *Biochemistry 46*, 424–435.
22. Kuznetsov, N. A., Koval, V. V., Zharkov, D. O., Nevinsky, G. A., Douglas, K. T., and Fedorova, O. S. (2005) Kinetics of substrate recognition and cleavage by human 8-oxoguanine-DNA glycosylase. *Nucleic Acids Res. 33*, 3919–3931.
23. Vallur, A. C., Feller, J. A., Abner, C. W., Tran, R. K., and Bloom, L. B. (2002) Effects of hydrogen bonding within a damaged base pair on the activity of wild type and DNA-intercalating mutants of human alkyladenine DNA glycosylase. *J. Biol. Chem. 277*, 31673–31678.
24. Biswas, T., Clos, L. J., II, SantaLucia, J., Jr., Mitra, S., and Roy, R. (2002) Binding of specific DNA base-pair mismatches by N-methylpurine-DNA glycosylase and its implication in initial damage recognition. *J. Mol. Biol. 320*, 503–513.
25. Vallur, A. C., Maher, R. L., and Bloom, L. B. (2005) The efficiency of hypoxanthine excision by alkyladenine DNA glycosylase is altered by changes in nearest neighbor bases. *DNA Repair 4*, 1088–1098.
26. Wyatt, M. D., and Samson, L. D. (2000) Influence of DNA structure on hypoxanthine and 1,N(6)-ethenoadenine removal by murine 3-methyladenine DNA glycosylase. *Carcinogenesis 21*, 901–908.
27. Hang, B., Sagi, J., and Singer, B. (1998) Correlation between sequence-dependent glycosylase repair and the thermal stability of oligonucleotide duplexes containing 1,N6-ethenoadenine. *J. Biol. Chem. 273*, 33406–33413.
28. Leonard, N. J. (1984) Etheno-substituted nucleotides and coenzymes: Fluorescence and biological activity. *CRC Crit. Rev. Biochem. 15*, 125–199.
29. O'Brien, P. J., and Ellenberger, T. (2003) Human alkyladenine DNA glycosylase uses acid-base catalysis for selective excision of damaged purines. *Biochemistry 42*, 12418–12429.
30. Rose, I. A., O'Connell, E. L., and Litwin, S. (1974) Determination of the rate of hexokinase-glucose dissociation by the isotope-trapping method. *J. Biol. Chem. 249*, 5163–5168.
31. Secrist, J. A.III, Barrio, J. R., Leonard, N. J., and Weber, G. (1972) Fluorescent modification of adenosine-containing coenzymes. Biological activities and spectroscopic properties. *Biochemistry 11*, 3499–3506.
32. Fersht, A. (1999) Structure and Mechanism in Protein Science , pp 200−201, W. H. Freeman and Company, New York.
33. Hsieh, J., Walker, S. C., Fierke, C. A., and Engelke, D. R. (2009) Pre-tRNA turnover catalyzed by the yeast nuclear RNase P holoenzyme is limited by product release. *RNA 15*, 224–234.
34. Baldwin, M. R., and O'Brien, P. J. (2009) Human AP Endonuclease I Stimulates Multiple-Turnover Base Excision by Alkyladenine DNA Glycosylase. *Biochemistry 48*, 6022–6033.
35. Maher, R. L., Vallur, A. C., Feller, J. A., and Bloom, L. B. (2007) Slow base excision by human alkyladenine DNA glycosylase limits the rate of formation of AP sites and AP endonuclease 1 does not stimulate base excision. *DNA Repair 6*, 71–81.
36. Kelley, S. O., and Barton, J. K. (1999) Electron transfer between bases in double helical DNA. *Science 283*, 375–381.
37. Riazuddin, S., and Lindahl, T. (1978) Properties of 3-methyladenine-DNA glycosylase from *Escherichia coli*. *Biochemistry 17*, 2110–2118.
38. O'Connor, T. R. (1993) Purification and characterization of human 3-methyladenine-DNA glycosylase. *Nucleic Acids Res. 21*, 5561–5569.
39. Wyatt, M. D., Allan, J. M., Lau, A. Y., Ellenberger, T. E., and Samson, L. D. (1999) 3-Methyladenine DNA glycosylases: Structure, function, and biological importance. *BioEssays 21*, 668–676.
40. de Prat Gay, G., Ruiz-Sanz, J., and Fersht, A. R. (1994) Generation of a family of protein fragments for structure-folding studies. 2. Kinetics of association of the two chymotrypsin inhibitor-2 fragments. *Biochemistry 33*, 7964–7970.
41. Schreiber, G., and Fersht, A. R. (1993) Interaction of barnase with its polypeptide inhibitor barstar studied by protein engineering. *Biochemistry 32*, 5145–5150.
42. Scharer, O. D., and Verdine, G. L. (1995) A designed inhibitor of base excision repair. *J. Am. Chem. Soc. 117*, 10781–10782.
43. Xia, L., Zheng, L., Lee, H. W., Bates, S. E., Federico, L., Shen, B., and O'Connor, T. R. (2005) Human 3-methyladenine-DNA glycosylase: Effect of sequence context on excision, association with PCNA, and stimulation by AP endonuclease. *J. Mol. Biol. 346*, 1259–1274.
44. Abner, C. W., Lau, A. Y., Ellenberger, T., and Bloom, L. B. (2001) Base excision and DNA binding activities of human alkyladenine DNA glycosylase are sensitive to the base paired with a lesion. *J. Biol. Chem. 276*, 13379–13387.
45. Huffman, J. L., Sundheim, O., and Tainer, J. A. (2005) DNA base damage recognition and removal: New twists and grooves. *Mutat. Res. 577*, 55–76.
46. O'Brien, P. J. (2006) Catalytic promiscuity and the divergent evolution of DNA repair enzymes. *Chem. Rev. 106*, 720–752.
47. Berti, P. J., and McCann, J. A. (2006) Toward a detailed understanding of base excision repair enzymes: Transition state and mechanistic analyses of N-glycoside hydrolysis and N-glycoside transfer. *Chem. Rev. 106*, 506–555.
48. Stivers, J. T., and Jiang, Y. L. (2003) A mechanistic perspective on the chemistry of DNA repair glycosylases. *Chem. Rev. 103*, 2729–2759.
49. Gerlt, J. A., and Babbitt, P. C. (2001) Divergent evolution of enzymatic function: Mechanistically diverse superfamilies and functionally distinct suprafamilies. *Annu. Rev. Biochem. 70*, 209–246.
50. Glasner, M. E., Gerlt, J. A., and Babbitt, P. C. (2006) Evolution of enzyme superfamilies. *Curr. Opin. Chem. Biol. 10*, 492–497.
51. Connor, E. E., and Wyatt, M. D. (2002) Active-site clashes prevent the human 3-methyladenine DNA glycosylase from improperly removing bases. *Chem. Biol. 9*, 1033–1041.
52. O'Brien, P. J., and Ellenberger, T. (2004) The *Escherichia coli* 3-methyladenine DNA glycosylase AlkA has a remarkably versatile active site. *J. Biol. Chem. 279*, 26876–26884.
53. Berdal, K. G., Johansen, R. F., and Seeberg, E. (1998) Release of normal bases from intact DNA by a native DNA repair enzyme. *EMBO J. 17*, 363–367.